THE EFFECTS OF INNER WAKE MODELLING ON BLADE AIRLOADS

R.H. Miller and S.C. Ellis
Massachusetts Institute of Technology
Cambridge, Massachusetts 02138 U.S.A.

and

L. Dadone
Boeing Helicopters
Philadelphia, Pennsylvania U.S.A.

Abstract

The higher harmonic airloads acting on rotor blades in forward flight are caused primarily by the interaction of the rotor with its own wake. In computing these airloads the wake may conveniently be modelled by assuming that the wake rolls up rapidly, well before encounter with a following blade, into discrete trailing vortex filaments whenever the slope of the bound circulation changes sign. Such modelling gives results in reasonable agreement with test data, particularly if a free wake is postulated. While there is some experimental evidence that a vortex rolls up rapidly from the blade tip, none appear to exist to substantiate the assumption of rapid roll-up of the inner wake. An analytical prediction of wake roll-up was therefore initiated which substantiated the existence of a tip vortex which rolled up rapidly, but cast doubt on the existence of discrete inner vortices, suggesting rather that this inner wake remains as a vortex sheet. Some of the results from this investigation are presented. The effects on the rotor blade airloads of differing assumptions as to the inner wake roll-up schedule are discussed.

Introduction

The nature of the vibratory airloads acting on a rotor depends to a great extent on the dynamics of wake formation. Of particular importance is the time required for a sheet of vorticity to roll up into discrete vortices, since the loads induced on a blade by a sheet of distributed vorticity are quite different from those induced by a vortex of equal strength. Also of importance is the location of the wake at the time of its encounter with a following blade.

The free wake analysis of Ref. 1 used the Betz criterion (Ref. 2) of conservation of momentum to find the spanwise locations of the inner and outer vortices formed from the maximum bound circulation on a blade in forward flight. In Ref. 3, Hooper analyzed existing experimental data and identified a small region of negative load near the tip of the blade on the advancing side of the rotor, at the higher forward speeds, as a possible reason for the inability of the then available codings to predict the extensive higher harmonic blade air loads. Ref.4 postulated that a sheet of vorticity could roll up whenever the rate of change of bound circulation changed sign, therefore, in Ref. 5, the wake trailed due to the change from a negative load at the tip, when it existed, to the maximum positive

load over the mid portion of the blade was modeled by a third vortex. The introduction of this third vortex resulted in a better agreement between theory and test. The most recent results, using a free wake, are given in Ref. 6. In all these analyses it was assumed that vortex roll-up was rapid and occurred well before encounter with a following blade.

Certain discrepancies remained, however, and it was decided to re-examine the assumption of rapid vortex formation, using the techniques discussed in Ref. 6. Conclusions from this investigation, given in greater detail in Ref. 7, will be briefly reviewed in this paper, together with results showing the effects of various assumptions as to the wake roll-up schedules on rotor loads prediction.

Wake Modeling

Of interest is the location, and the degree of roll-up, of a sheet of vorticity trailed by a blade at the time of its encounter with a following blade. A time marching model was therefore used, as described in Ref. 6, with the sheet modeled by a series of vortex filaments. The time history of roll-up was computed over time intervals corresponding to those required for following blades to encounter this wake.

There is an extensive body of literature on wake roll-up, mostly of the wake generated by an elliptically loaded wing. One of the earliest examples is the work of Westwater, Ref. 8, using a filamentary wake representation. Wake interferences as time progressed, and increasingly chaotic motions as discretization was increased, resulted in attempts to improve the modeling, for example by "core dumping" and rediscretization after a number of steps. Ref. 9 contains a useful review of this literature, with examples showing the improvements in roll-up geometry made possible by these and similar techniques.

Since the concern in Ref. 7 was with establishing the general nature of the inner wake roll-up and its migration, detailed modeling of the core structure was of secondary importance. Consequently, the simple time marching model was used without further refinement other than to introduce a measure of coalescence, that is, the assumed merging of any two vortex filaments which approached closer than a specified distance. Allowing coalescence results in a somewhat better representation of the behavior of the physical wake generated by a lifting surface and serves to highlight the centroid of the rolling-up vortex while somewhat alleviating the erratic behavior previously noted.

Ideally the core size should be varied with time as determined by the conservation of kinetic energy. This was done for the hovering case in Ref. 10 but is clearly a more complex procedure in the case of a filamentary model and for forward flight. Conservation laws also apply to coalescence; however, the effects of varying both the core size and coalescence were shown to have a relatively minor effect on the overall wake geometry of interest here and such additional refinements were therefore not attempted.

Wake Geometry

Figure 1 shows the geometry of the wake generated from the tips of a four-bladed rotor with the blades at various azimuth positions, ψ, at an advance ratio of $\mu = 0.4$. The encounter at $\psi = 80$ deg. causes most of the peak higher harmonic loadings. At this azimuth, encounter occurs with a

wake trailed by the immediately preceding blade (90 deg. ahead for a four-bladed rotor), and born at 105 deg. Hence its age is 65 deg., corresponding in this case to a time increment of 0.05 seconds. As discussed in Ref. 6, information on the wake in the vicinity of $\phi = 105$ deg is all that is required in order to predict the effects of wake dynamics on the higher harmonic blade loads to a high degree of accuracy. Figure 2a sketches the distribution of bound circulation which generated this wake, showing the characteristic negative peak near the tip of the blade noted by Hooper. This distribution has been used for most of the studies discussed in this paper.

Figures 1b to 1d show the nature of the encounters on the retreating side. No encounters occur at 280 deg. At 300 deg. the target blade first encounters the wake generated from the tip of the preceding blade at $\phi = 240$ deg. The wake thus has an age at encounter of 150 deg., appreciably older than that for encounters on the advancing side. At $\psi = 320$ deg. encounter occurs with a wake born at 200 deg. and hence with an age of 210 deg. The vortex remains over the outer 70% of the blade until it leaves the blade at about $\psi = 20$ deg. with an age of 240 deg. The loadings of interest are thus those occurring on the advancing side at about 100 deg. and on the retreating side at 200 deg. to 400 deg. with ages on the advancing side of less than 200 deg. and on the retreating side of about 200 deg. The bound circulation distributions for the retreating side are shown in Figs. 2b to 2d.

The bound circulation distributions shown in Fig. 2 were computed using nine spanwise stations on the blade, corresponding to the stations used for the experimental results with which the computed results are later compared.

Ref. 7 contains results from an extensive series of calculations using these, and similar, loadings. These studies showed that the tip vortex rolls up rapidly as assumed and that the vertical location of this vortex at encounter with a following blade is reasonably well estimated without the need to refine the wake spatial discretization beyond the nine stations used in the loads computations. Figure 3 shows the wake displacements after 100 deg. and 200 deg. using this "coarse" wake representation. There is no evidence of roll-up except at the tip, where the first point shown contains the strong tip vortex.

In order to explore the effects of discretization, a splining technique was used to generate a much finer wake with an initially uniform spacing of .01 of the blade span. The resulting wake structure is shown in Fig. 4. Again, no evidence of mid span roll-up is evident at an age of 100 deg. At 200 deg. a tendency to roll-up is apparent at about the 85% span point, close to the location computed in the loads program discussed above. However, the amount of circulation involved is only a fraction of that which previously had been postulated for the mid vortex.

In order to clarify the activity over the important outer 50% of the blade, the wake was refined further, to a trailed filament spacing of 0.005 of span, and the time step used was reduced from an equivalent azimuth change of 20 deg. to one of 4 deg. The scale of the graphics was also increased and only the outer 50% of the blade was modeled. The results are shown in Fig.5. At 200 deg. the definition of the tip vortex has improved but, as before, there is no evidence of a mid vortex roll-up. At 200 deg. there is clear evidence of such a roll-up, but again the circulation involved is

considerably less than that postulated for the mid vortex in the loads programs. Some of the vorticity expected in this vortex appears as distributed vorticity around the tip vortex, most of the rest remaining in the sheet. Table I shows the postulated vorticity, I/R, of the tip and mid vortices used in the loads programs, compared with the strengths associated with the roll-ups evident in fig. 5. Some coalescence is indicated by the breaks in Fig. 5 near the tip, and at 85% span.
The computations were for an age of 200 deg. and the loading of Fig. 2a

Table I Tip and mid vortex strength

	Tip vortex	Mid vortex
From loads program	0.0170	0.042
From computations of Fig. 6	0.0175	0.00437

On the retreating side the results were similar, as shown in Fig. 6, based on the loading of Fig. 2d. There was little evidence of inner wake roll-up, in this case not unexpectedly, nor was one postulated in the loads program except near the root.

It is evident that the model fails to predict any appreciable inner wake roll-up. At an age of 200 deg. some roll-up is evident, but the vortex strength is far below that assumed. On the retreating side the tip vortex is reasonably well predicted but, rather than rolling up into a root vortex, the inner wake appears to remain essentially as a sheet of vorticity with only minor indications of roll-up.

Visualization of the inboard vortex sheet at conditions other than hover has always been difficult. Over the years many attempts to visualize the rollup of the inboard vorticity have been made: most of them unsuccessful and unreported... An unsuccessful but reported attempt is presented in Ref. (14). This was a wake visualization test on a reduced scale model of the H-34 rotor, Ref. (11). The test was carried out in water, in a towing tank. While ample evidence was obtained on the rollup of tip vortices, due to both positive and negative loading, no evidence was seen of any inboard rollup of the vortex sheet. At the time it was speculated that the low Reynolds number environment may have compromised an already light load distribution, but the present calculations show that the spanwise gradients in bound circulation may have been too small to promote vortex sheet rollup independently of any scale effect.

The conclusion is either that the filamentary wake model used is inadequate for computing wake dynamics, or that the inner wake does not roll up, remaining essentially as a sheet.

Rotor Blade Loads

Methods for computing blade airloads in forward flight have been developed by several investigators. The fast free wake technique of Ref. 5 is a convenient method for rapidly examining the effect of various hypotheses and determining the sensitive parameters in the calculations. This model is based on the well-validated assumption that the wake geometry need only be accurately defined where a blade vortex interaction occurs, with the rest of the wake being approximately modeled, in this case by doubly infinite line vortices. In the models of Ref. 6 it was assumed that the wake rolled up, before first encounter, into vortices whose strengths were determined by the absolute maxima of the

bound circulation on the blade. When two, or more, such maxima occurred, as on the advancing side (see Fig. 2a), additional vortices were added. The spanwise location of the rolled-up vortices were determined by the first moment of the vortex filaments forming each rolled-up vortex. The results showed good agreement between the experimental and theoretical higher harmonic airloads over the outer portions of the blade, where most of the higher harmonic activity occurs. However, there was appreciably more harmonic loading over the inner sections than was indicated by the experimental data.

Also, the assumption that the vortex sheet is immediately rolled up causes the rotor codes to calculate blade/wake proximity airload "signatures" (loading spikes due to the assumed vicinity of concentrated vortices) which are not substantiated by experiment. This disagreement between test and theory was not fully quantifiable in the H-34 data, which were digitized manually at relatively coarse increments, but it has been looked into in more detail in more recent tests, such as the Model 360 test at DNW, (Ref. 13). The standard fix for this is the assigning of a large vortex "core" which reduces, arbitrarily, the locally induced velocities, as discussed below.

As in other studies, the validity of the theoretical models was checked by comparison with the full scale rotor test data reported in Ref. 11, probably the only comprehensive series available. Comparisons were made by visual inspection of both the total and the higher harmonic airloads (above the second harmonic) and by direct comparison between the experimental and computed airloads at various spanwise stations.

Figure 7 shows the map of the experimentally determined airloads in three dimensions. The vertical axis represents the airloads, in lbs/in, the horizontal axis the azimuth, ψ, and the third dimension the blade span. The projection is thus of the "Mercator" type in which the root section circumferential displacements have been expanded to equal those at the rotor tip. Data for the tip section, at 99% span, have not been included since the loads are small at this station and, due to the limitations of the graphics used, their inclusion tends to mask the more important loads starting at the 97% span station. In Fig. 7 both the total loads and those primarily wake-induced (above the second harmonic) are shown.

Figure 8 shows similar projections for the analytical results obtained with a free-wake program similar to that of Ref. 6. A quantitative comparison between the computed and measured loading at any station may best be made by plotting the two values together, as shown in Fig. 9. More complete results are given in Ref. 6.

Figures 10 and 11 show the results obtained when the mid vortex is replaced by a sheet of distributed vorticity. For the purpose of this analysis, the sheet was taken as extending from the maximum negative loading near the tip, shown in Fig. 2a to the maximum positive loading close to mid span, and was assumed to be of uniform strength. This is equivalent to assuming that the slope of the bound circulation shown in Fig. 2a was constant between these two peaks. The peak higher harmonic loads near the 90 deg. azimuth are somewhat reduced compared to the experimental data and to the analytical results shown in Fig. 9, although the total loads are in somewhat better agreement with the experimental values. However,

the changes are in general small, despite the significantly lower velocities induced by the ccombined vortex sheet and tip vortex model of the far wake.

Table II: Induced velocities for $\eta = 0.90$ and $\psi = 80°$

	no inner wake	inner wake
far wake	-0.0104	-0.0191
near wake	-0.0022	0.0052
shed wake	-0.0049	-0.0030
total	-0.0175	-0.0168

An approximate method for representing a sheet of vorticity, suggested in Ref. 12, is to assume that the mid vortex has a very large core of the order of 20 to 30% of the span. A more drastic step is to eliminate the mid vortex entirely, whether represented by a single vortex or a sheet. Both these methods gave results essentially identical to those discussed above. Accordingly, the model of Ref. 6 was used to investigate the individual contributions of various wake elements to induce airloads. Figure 12 shows clearly that only small changes result in the induced loading when the inner wake model is changed. In particular, there is almost no difference between the 2 models in predicting peak induced loads ($\eta = 0.90$, $\psi = 80°$). In contrast, the portion of induced air loads due to the far wake is shown in Figure 13. The large change in the peak values at $\psi = 80°$ is shown clearly. Upon examining the individual velocities induced by each component of the wake (Table II), it is evident that the velocity induced by the near wake also changes significantly. A plot of the blade bound

circulation (Figure 14) for the 2 models shows that changes in the near wake contribution are due to a significant change in bound circulation along the blade. These changes are due to relatively large effect of the inner wake vortex intersecting the blade at the 0.87 radial station.

Concluding Remarks

The higher harmonic airloads on a rotor occurring in high speed forward flight are determined primarily by the changes in strength with azimuth of the tip vortex, and are relatively insensitive to inner wake modeling.

The modeling of BVI events cannot be meaningfully accomplished without the correct definition of vortex sheet rollup. While the prediction of tip vortex rollup can be carried out fairly easily, populating the inboard wake with a number of arbitrarily rolled up vortices can produce a erroneous picture. It is true that in the impingement of the wake on the blades other phenomena have to be modelled (close interactions, viscous effects, etc.,) but the next level of complexity in wake modelling should not be undertaken until the basic "free" wake is physically correct.

Both in the wake modeling for comprehensive (standard lifting line and surface) rotor airloads codes, the emphasis must be on the mechanism and extent of wake rollup (in the highly specialized rotor environment, straight wing Betz criteria are not adequate), and on the close interaction of the blades with the partially rolled up vortex sheets.

A full CFD treatment of the problem may shed some additional light where tests data is viry difficult to obtain, but any practical

design applications require a less computer intensive approach, which focuses on the most important features of the vortex sheet rollup in rotor environment.

References

1. Scully, M. Computation of helicopter rotor wake geometry and its influence on rotor harmonic airloads, MIT ASRL TR 178-1, March 1975.

2. Donaldson, C., Snedeker, R.S. and Sullivan, R.D. Calculation of the wakes of three transport aircraft in holding, takeoff, and landing configurations, and comparison with experimental measurements, AFOSR-TR-73, 1954.

3. Hooper, W.E. The vibratory airloading of helicopter rotors, Vertica Vol. 8, No. 2, 1984.

4. Rossow, V. On the inviscid rolled-up structure of lift generated vortices, J. Aircr., Nov. 1973.

5. Miller, R.H. Factors influencing rotor aerodynamics in hovering and forward flight, Vertica, Vol. 9, No. 2, 1985.

6. Miller, R.H., Ellis, S.C., Dadone, L. The effects of wake migration during roll-up on blade airloads, Vertica, Vol. 113 No. 1, 1989.

7. Miller, R.H. Research on the dynamics of a curved wake, MIT CFDL TR-89-6 prepared for Boeing Helicopters, June 1989.

8. Westwater, F.L. A.R.C. R. & M. No. 1972, 1935.

9. Kantels, J.P. Calculation of asymmetric sheet roll-up, MIT MSc. Thesis, 1986.

10. Landahl, M.T. Roll-up model for rotor wake vortices, FFA HU 2262, 5, 1981. Also MIT ASRL TTL 194-4. See also Chung, S.Y. MIT PhD Thesis, 1986.

11. Rabbot, J.P., Lizak, A.A., Paglino, V.M. A presentation of measured and calculated full scale aerodynamic and structural loads, USS AVLAS T.R. 66-31, 1966.

12. Johnson, W. Comparison of calculated and measured model rotor loading and wake geometry, NASA TM 81189, 1980.

13. Dadone, L., Dawson, S., Boxwell, D., Edquist, D., "Model 360 Rotor Test at DNW - Review of Performance and Blade Airload Data", presented at the 43rd Annual Forum of the American Helicopter Society, St. Louis Mo., May 1987.

14. Jenks, M., Dadone, L., Gad-el-Hak, M., "Towing Tank Flow Visualization Test of a Model Scale H-34 Rotor", presented at the 43rd Annual Forum of the American Helicopter Society, St. Louis, Mo., May 1987.
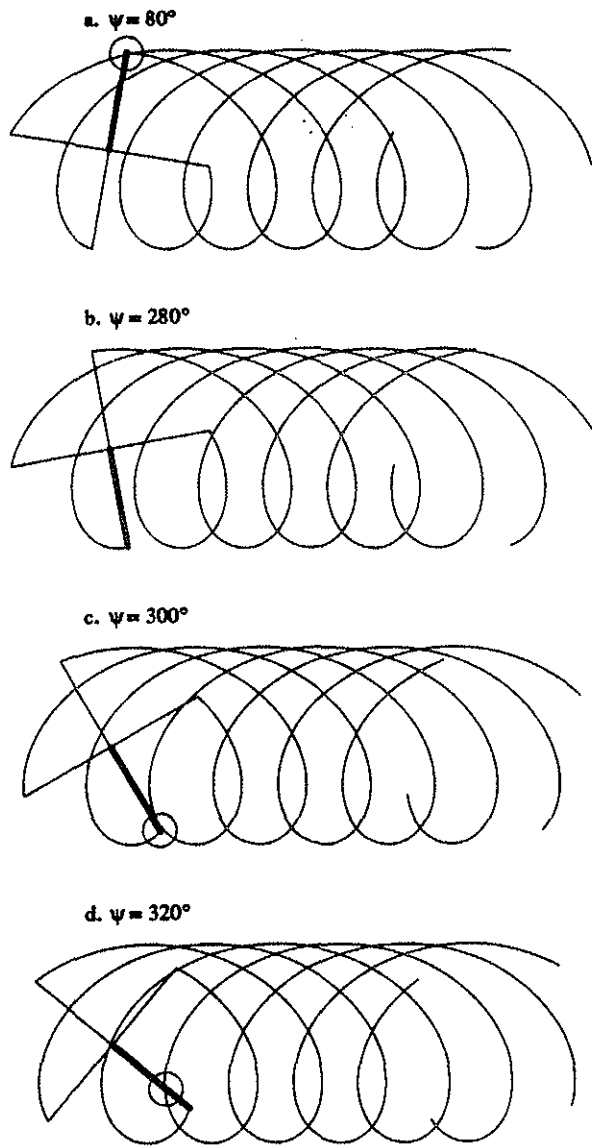
a. ψ = 80°

b. ψ = 280°

c. ψ = 300°

d. ψ = 320°

Fig. 1. Wake geometries at various azimuth positions

$\psi = 100°$
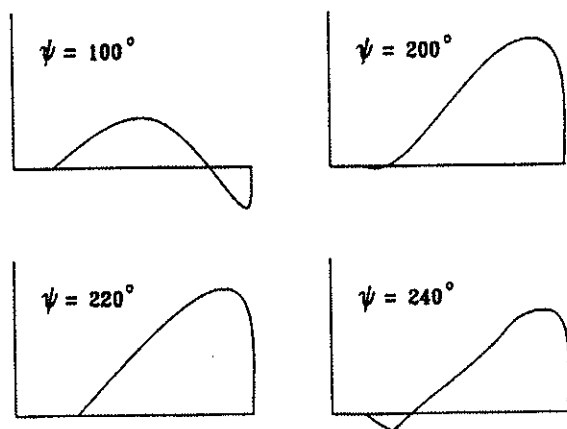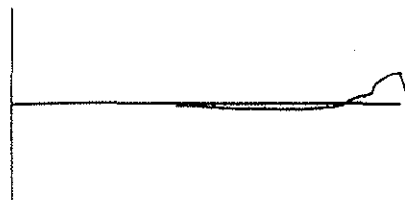
$\psi = 200°$

$\psi = 220°$

$\psi = 240°$

Fig. 2. Spanwise distribution of bound circulation at various azimuth positions
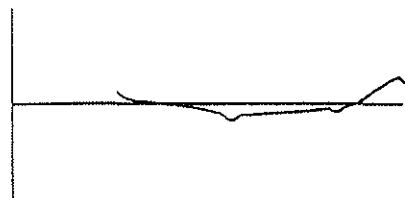

Geometry of wake roll-up at an age of 100 degrees

Geometry of wake roll-up at an age of 200 degrees

Fig. 3. Wake geometries using a nine-trailer wake model with the loading of Fig. 2a and a timestep of 20 deg. azimuth change

Geometry of wake roll-up at an age of 100 degrees

Geometry of wake roll-up at an age of 200 degrees

Fig. 4. Wake geometries predicted using a 100 trailer wake, dr = 0.01R, and a time step of 20 degrees

Geometry of wake roll-up at an age of 100 degrees
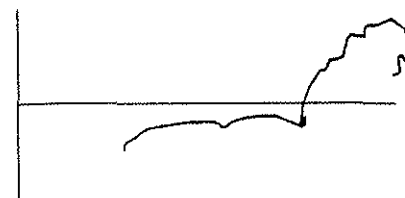
Geometry of wake roll-up at an age of 200 degrees

Fig. 5. Wake geometries over outer 50% of blade with dr = .005R and a time step of 4 degrees

Geometry of wake roll-up at an age of 100 degrees

Geometry of wake roll-up at an age of 200 degrees
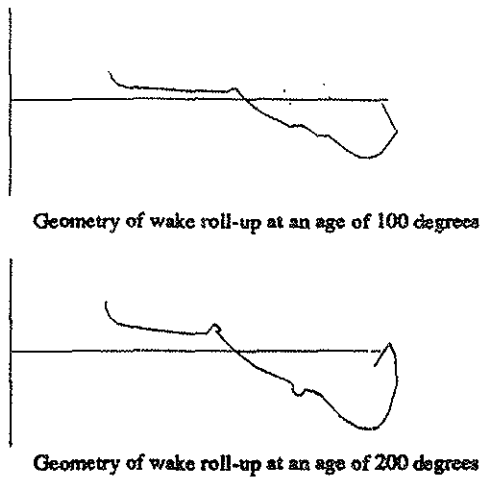
Fig. 6. Wake geometries on the retreating side of the rotor, using the loading of Fig. 2d, dr = 0.01R and a time step of 20 deg.
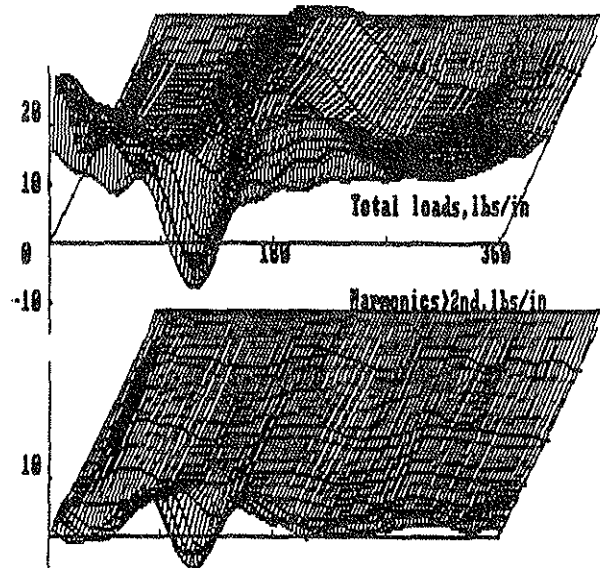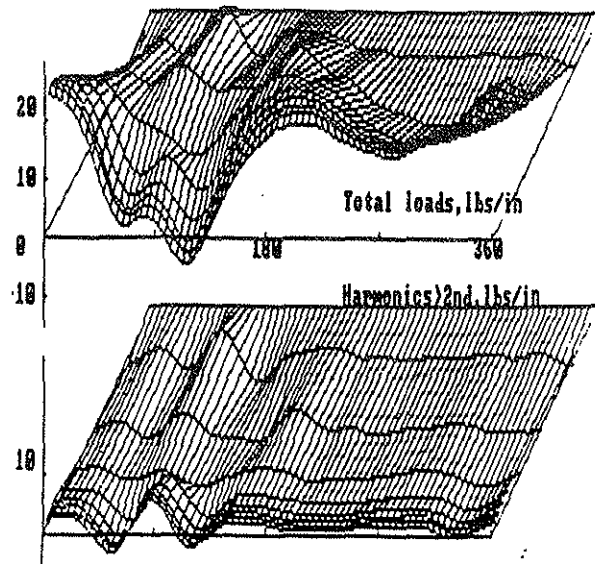

Total Airloads
Rolled up inner wake

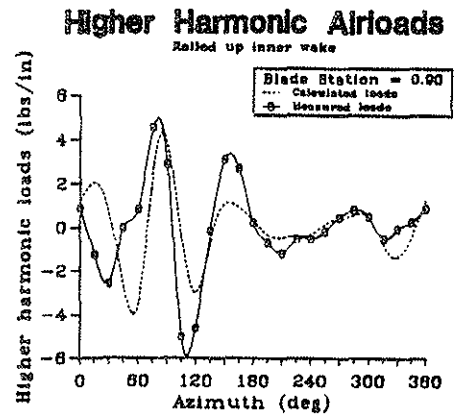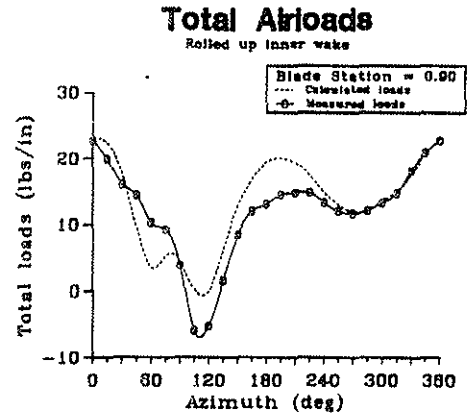
Higher Harmonic Airloads
Rolled up inner wake

Fig. 9. Comparison of computed and experimental airloads at 90% span Rolled up inner wake

Fig. 7. Map of airloads from the experimental results of Ref. 11
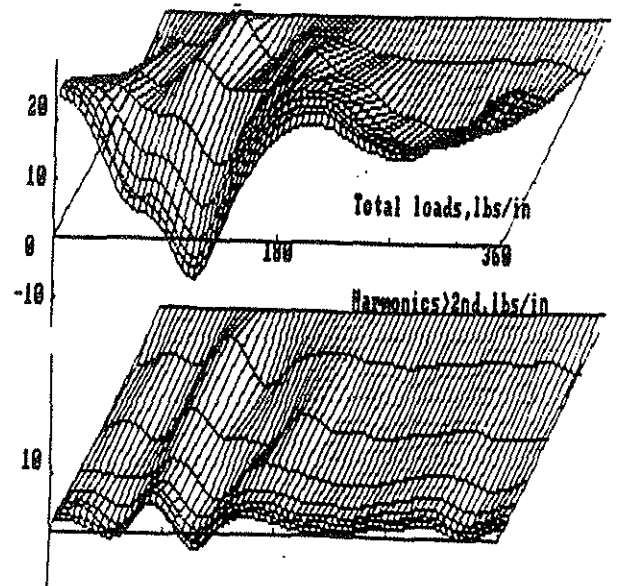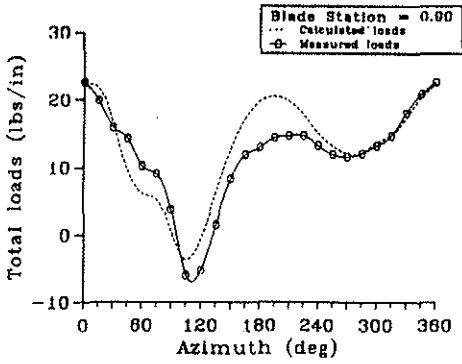

Fig. 8. Map of computed airloads with a rolled up inner wake

Fig. 10. Map of computed airloads with vortex sheet inner wake model

Total Airloads
Vortex sheet inner wake

Blade Station = 0.90
··· Calculated loads
-⊖- Measured loads

Total loads (lbs/in)

Azimuth (deg)

Far Wake Induced Loads
blade station = 0.90

···· Inner vortices incl.
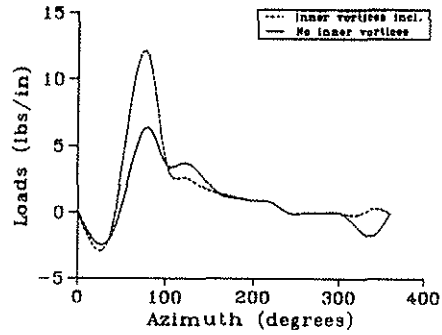—— No inner vortices

Loads (lbs/in)

Azimuth (degrees)

Fig. 13. Comparison of far wake contribution to airloads, with and without rolled up inner vortices
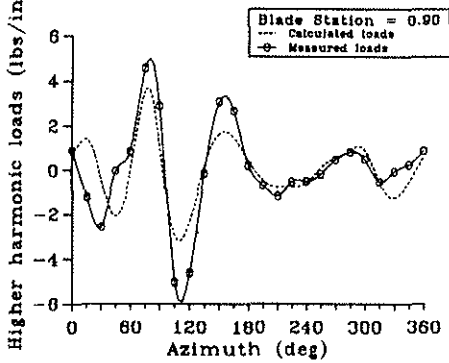
Higher Harmonic Airloads
Vortex sheet inner wake

Higher harmonic loads (lbs/in)

Blade Station = 0.90
··· Calculated loads
-⊖- Measured loads

Azimuth (deg)

Fig. 11. Comparison of computed and experimental airloads at 90% span for vortex sheet inner wake.
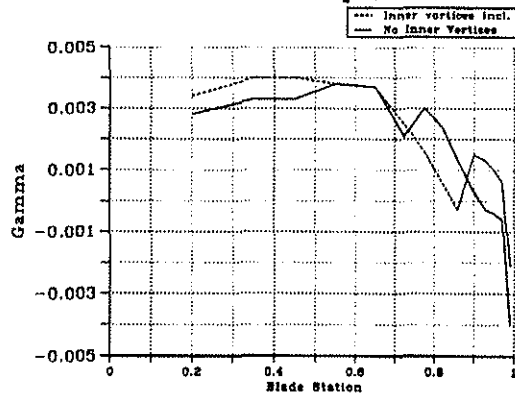
Blade Bound Circulation
Psi = 60 degrees

···· Inner vortices incl.
—— No inner vortices

Gamma

Blade Station

Fig. 14. Comparision of blade bound circulation with and without rolled-up inner wake

Total Induced Airloads
blade station = 0.90

···· Inner vortices incl.
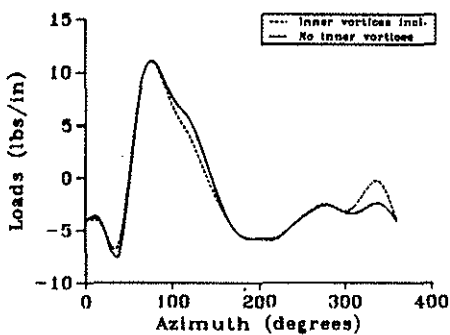—— No inner vortices

Loads (lbs/in)

Azimuth (degrees)

Fig. 12. Comparison of wake induced loads with and without inner wake vortices